distances (interatomic distances) from a surrounding transition metal in an octahedral site and a tetrahedral site. Once a desired bias was applied at a NCO-HNS electrode, the second FT peak from single-scattering of Ni-Co path decreased relative to the unbiased condition (Fig. 2(c); Ni K-edge), which could be attributed to the partial oxidation of Ni cations, and further revealed the observation from X-ray-absorption near-edge structure of the Ni K-edge. In terms of Co cations, there was no considerable change with and without applied potential, which indicates that Ni cations acted as more active roles than Co cations in OER. Nevertheless, the role of Co on the surface of NCO-HNS during water oxidation cannot be totally excluded as a more active property of the Ni cation might result from a local environment generated by coordinated Co cations and oxygen anions. Furthermore, Co oxide might also act as a scaffold to provide a conductive matrix for charge carriers. The X-ray absorption spectral data revealed that enriched Ni^{3+} on the surface of NCO-HNS was consequently, more active than Co to initiate the formation of NiOOH and was responsible for most redox sites acting for OH^- adsorption in an alkaline solution, which was critical to enhance OER.

In summary, their observations demonstrated a strong correlation between the initialization of oxygen evolution and the formation of an active metal-oxide phase. The X-ray technique *in situ* provides a powerful tool to investigate the phase of a surface-active metal centre in electrocatalysis and can be potentially applied to probe other catalytic systems. In practical applications, solar splitting of water or artificial photosynthetic devices can be achieved through integration of a reliable catalytic system with a photovoltaic solar cell, which captures radiant energy to generate a sufficient driving force for H_2/O_2 generation. (Reported by Yan-Gu Lin)

This report features the work of Hao-Ming Chen and his co-workers published in Nat. Commun. ***6****, 8106 (2015) and Adv. Energy Mater.* ***5****, 1500091 (2015).*

References

1. C. W. Tung, Y. Y. Hsu, Y. P. Shen, Y. Zheng, T. S. Chan, H. S. Sheu, Y. C. Cheng, and H. M. Chen, Nat. Commun. **6**, 8106 (2015).
2. H. Y. Wang, Y. Y. Hsu, R. Chen, T. S. Chan, H. M. Chen, and B. Liu, Adv. Energy Mater. **5**, 1500091 (2015).

Iron Titanate Kicks Off the Photogenerated Hole

Hematite is an effective photocatalyst for solar oxidation of water because of its favorable optical band gap (2.1–2.2 eV), low cost, abundance, and chemical stability in an oxidative environment. Its practical performance for solar water oxidation is, however, still poor owing to various factors such as improper band-edge position, poor conductivity, poor reaction kinetics of oxygen evolution, and short hole-diffusion length (2–4 nm). Many efforts have been made to improve the performance of hematite photoelectrodes. Ti-based treatments have also been widely used and effective methods to improve the performance of hematite photoanodes. Ti-based coating on hematite was shown to enhance effectively the performance with an obvious cathodic shift of the onset potential and an increased photocurrent. Ti-doping in hematite via various approaches such as atomic-layer deposition, deposition annealing or sol-flame synthesis, has also been widely used to improve the performance of hematite by increasing photocurrent and decreasing onset potential. Numerous mechanisms have been proposed to explain the effect of Ti-based treatments. Among them, Ti substitution of Fe in hematite (the formation of $FeTiO_3$ with Fe^{2+}) with improved donor density has been widely reported, but the improved photoactivity of Ti incorporation in hematite could be not simply attributed to the enhanced conductivity. Meanwhile, no Fe^{2+} signal was found in various Ti-treated hematite nanostructures. Mechanism of a Ti-based treatment was hence still an open question.

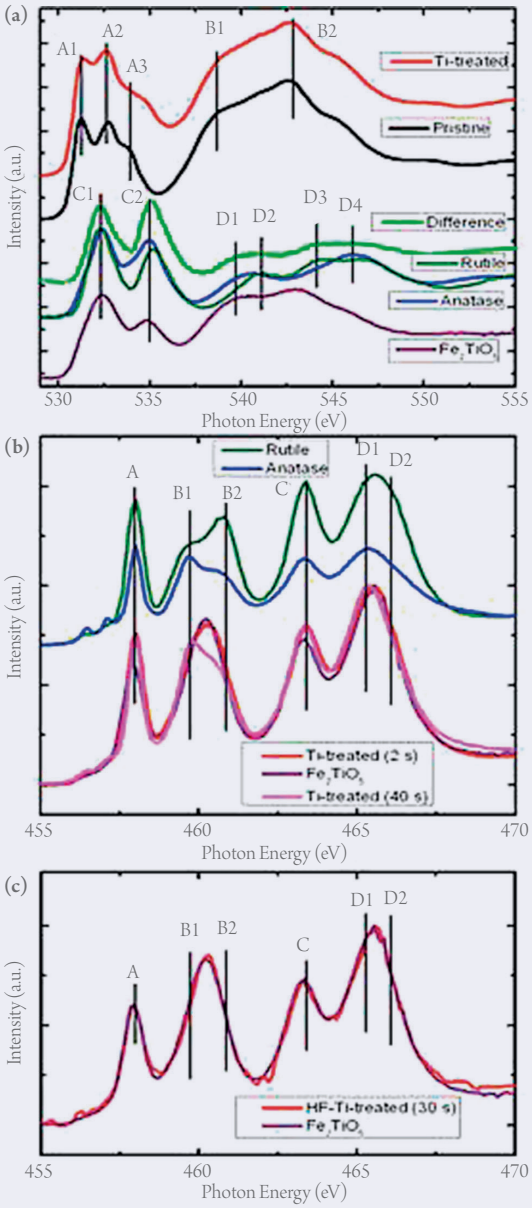

Fig. 1: (a) O K-edge XAS of pristine and Ti-treated (2 s) hematite nanostructures compared with spectra of rutile TiO_2, anatase TiO_2 and Fe_2TiO_5. The difference spectrum between the pristine and Ti-treated hematite is also shown. (b) Ti L-edge XAS of Ti-treated (2 and 40 s) hematite nanostructures compared with the spectra of rutile TiO_2, anatase TiO_2, and Fe_2TiO_5. (c) Ti L-edge XAS of HF-Ti-treated (30 s) hematite nanostructures compared with the spectrum of Fe_2TiO_5. [Reproduced from Ref. 1]

Xuhui Sun (Soochow University, China), Jun Zhong (Soochow University, China) and Shuit-Tong Lee (Soochow University, China) recorded cooperatively synchrotron-based soft X-ray absorption spectroscopy (XAS) at **BL20A1** to explore the electronic structure and chemical state of hematite nanostructures before and after Ti treatment.[1] XAS implies the excitation of electrons from a core level to local and partial empty states, which is an effective tool to probe the electronic states of complicated materials. Two Ti treatments of hematite were used in their work; FeOOH on a FTO substrate was prepared with a hydrothermal method. One type of Ti treatment was to evaporate a $TiCl_4$ solution on the surface of FeOOH

with subsequent annealing (labeled as Ti-treated hematite). The other way was a HF-assisted Ti treatment on immersing FeOOH into a Ti-dissolved HF solution with subsequent annealing (labeled as HF-Ti-treated hematite).

Figures 1(a) and 1(b) show O K-edge and Ti L-edge XAS of pristine and Ti-treated samples, respectively. In Fig. 1(a) the O K-edge spectrum of the pristine sample exhibits three separate prepeaks (A1-A3) and two main peaks (B1 and B2). Prepeaks A1 and A2 were attributed to typical hematite features related to transitions to antibonding O 2p states hybridized with Fe 3d states. Main peaks B1 and B2 were assigned to oxygen 2p states hybridized with Fe 4s and 4p states. An additional peak A3 was also observed, which might be attributed to carbon contamination. The spectrum of Ti-treated hematite showed features similar to those of pristine hematite, but the peak intensities differed from those of pristine hematite because of the Ti-based coating layer. To clarify the electronic structure of the coating layer, they show a magnified difference spectrum (Ti-treated hematite minus pristine hematite, with the spectrum of Ti-treated hematite normalized to ensure that the difference spectrum had no negative value) and compared it with some reference spectra in Fig. 1(a). The difference spectrum clearly showed a similar spectral shape to that of rutile and anatase TiO_2 with two prepeaks (C1 and C2) and four peaks labeled D1-D4 at higher energies. Although the difference spectrum resembled that of rutile and anatase TiO_2, it was not the same as either of them: D3 was more intense than D4, similar to that of rutile TiO_2, whereas the intense peak D1 showed a similar shape to that of anatase TiO_2. The intense D1 peak could also be from Fe_2TiO_5 (shown as a reference spectrum), but, because of the strong influence from hematite underneath at the O K-edge, it is difficult to identify the composition of the Ti-based coating layer from only the difference spectrum.

The Ti L-edge XAS signal came from only the coating layer of the sample and could be used to identify the composition. The Ti L-edge spectra of Ti-treated hematite and some reference samples are shown in Fig. 1(b). The reference spectra of rutile and anatase TiO_2 show clear main peaks A-D. Peaks A and B (B1 and B2) were attributed to Ti L_3-edge features, whereas peaks C and D (D1 and D2) were attributed to Ti L_2-edge features. For both Ti L_2 and L_3 edges, the crystal-field splitting of the 3d band produced t_{2g} (peaks A and C) and e_g (peaks B and D) subbands. It is also worth noting that, for both rutile and anatase TiO_2, the eg-related peaks (B and D) split further into two peaks, as shown in Fig. 1(b), labeled B1, B2, D1 and D2. The splitting of peak D into D1 and D2 was poorly resolved because of the lifetime-related broadening of the L_2 edge. The Ti-treated (2 s) hematite sample showed a spectral shape similar to that of rutile or anatase TiO_2, but doublet peaks B1 and B2 disappeared and a single peak was located between B1 and B2 in the Ti-treated (2 s) sample. This indicates that the Ti-based coating layer (2 s) on hematite was neither rutile nor anatase TiO_2. Interestingly, the spectrum of the Ti-treated (2 s) hematite was almost identical to that of Fe_2TiO_5 except for a different intensity of peak A; in particular, a single peak B appeared at the center between peaks B1 and B2. The resemblance of the two spectra indicates that the coating has the Fe_2TiO_5 structure, In recent reports, amorphous TiO_2 was also suggested to be an effective component for solar oxidation of water in Ti-treated hematite. Although amorphous TiO_2 also had a single peak B without the doublet structure of B1 and B2 according to previous XAS results, the energy of peak B for amorphous TiO_2 was located closer to peak B1. This is significantly different from their result, where peak B is located at the energy between peaks B1 and B2. The data strongly indicate that the coating layer on hematite has Fe_2TiO_5 structure.

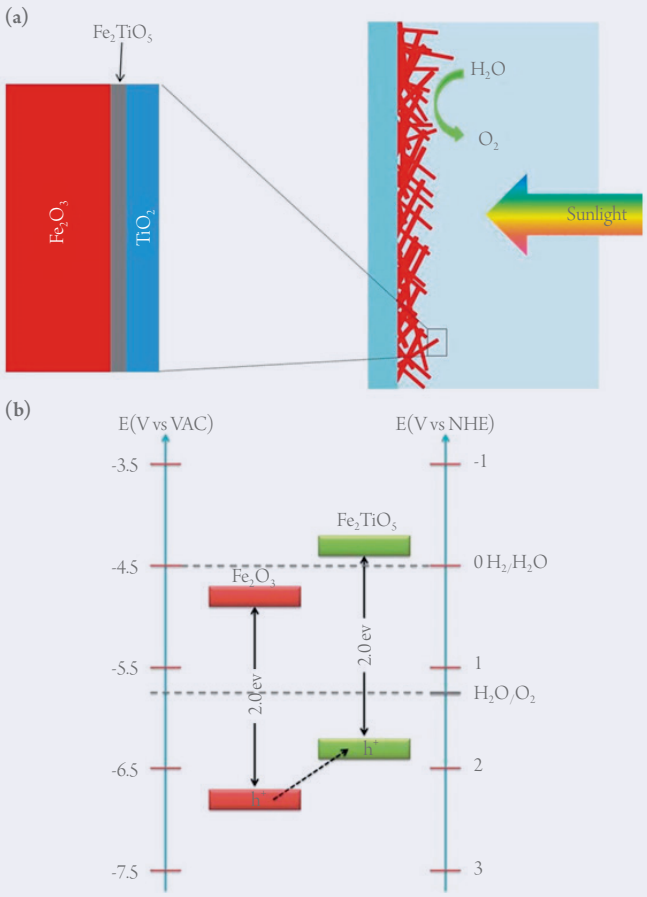

Fig. 2: (a) Illustration of compositions in Ti-treated hematite. (b) Band structure of Fe_2TiO_5 and hematite. [Reproduced from Ref. 2]

In the Ti-treated process with $TiCl_4$, TiO_2 could be formed on FeOOH during the exposure, but, further annealing at a temperature beyond 500 °C might introduce a Fe_2TiO_5 structure when TiO_2 reacted with hematite. The surface layer of Fe_2TiO_5 formed a heterojunction structure with hematite due to a favorable band structure. Figure 2(a) shows the compositions in Ti-treated hematite. The band structures of Fe_2TiO_5 and hematite are shown also in Fig. 2(b). The band gap of the Fe_2TiO_5 sample was estimated as about 2.0 eV by UV-visible spectrum. Ultraviolet photoelectron spectroscopy were used to measure the top of the valence band (VB, about -6.31 eV compared to the vacuum level). The band structure of their Fe_2TiO_5 sample was thus obtained in Fig. 2(b) (0 V vs RHE equals -4.5 V vs vacuum). The top of the VB of Fe_2TiO_5 was clearly higher than that of hematite, which favored the hole transport from hematite to Fe_2TiO_5 and a decreased photoexcited hole accumulation on the surface of hematite. The performance was thus improved with the heterostructure of Fe_2TiO_5 and hematite. The formation of the Fe_2TiO_5-hematite heterostructure might also explain the thickness effect of the coating layer. As the duration of treatment increased, a thicker coating layer was produced on hematite, but the increased part could not react with hematite to produce further Fe_2TiO_5. Formation of the top layer of TiO_2 would not help the water oxidation; instead it might decrease the photoabsorption, leading to decreased performance. The Ti L-edge XAS of a Ti-treated hematite sample after a treatment for 40 s is also shown in Fig. 1(b). A different peak B with doublet peaks B1 and B2 (B1 is higher than B2, indicatng anatase TiO_2) was observed, indicating that the top layer after long exposure of $TiCl_4$ is TiO_2.

The Ti L-edge spectrum of HF-Ti-treated (30 s) hematite with an ultrathin Ti-based layer is shown in Fig. 1(c), compared with the spectrum of Fe_2TiO_5. Similar to $TiCl_4$-treated hematite, HF-Ti-treated (30 s) hematite showed a

single peak B located between peaks B1 and B2. This indicates the formation of Fe_2TiO_5. The spectra of $TiCl_4$-treated hematite and Fe_2TiO_5 showed a slight difference in the intensity of peak A, attributed to the existence of TiO_2 in the top layer, but the spectra of the HF-Ti-treated (30 s) sample and Fe_2TiO_5 were almost identical because of the ultrathin layer. When the FeOOH sample on an FTO substrate was immersed in Ti-dissolved HF solution, Ti ions adsorbed on the surface of FeOOH; the etching of FeOOH by HF might favor this process. The following annealing in air produced amorphous TiO_2, which reacted with hematite to form an ultrathin layer of Fe_2TiO_5. The Fe_2TiO_5-hematite heterostructure was thus formed to yield satisfactory performance.

In summary, it is revealed by XAS measurment that Fe_2TiO_5 forms a heterojunction with hematite. This heterojunction decreases the photogenerated hole accumulation and improves the performance of hematite. The facile synthesis of the new heterojunction structure became an effective method to improve the performance of hematite for solar oxidation of water. The new Fe_2TiO_5-hematite heterostructure provides insight into understanding the enhanced performance of other Ti-treated hematite nanostructures. (Reported by Yan-Gu Lin)

This report features the work of Xuhui Sun and his co-workers published in ACS Nano ***9****, 5348 (2015).*

Reference

1. J. Deng, X. Lv, J. Liu, H. Zhang, K. Nie, C. Hong, J. Wang, X. Sun, J. Zhong, and S. T. Lee, ACS Nano **9**, 5348 (2015).

Zoom in the Perovskite Solar Cell with X-ray Scattering

Organometal halide-perovskite solar cells attract considerable attention because of their advantages of high performance, low cost, processability in solution, light weight and flexibility. Such perovskite solar cells demonstrate an exciting progress with efficiency of power conversion (PCE) up to 19.3 %. The structure of the perovskite film, generally characterized according to the uniformity, coverage and pin-hole (or gap) between grains, is the critical role strongly affecting the PCE. The crystalline characteristics of the perovskite layer were reported to play important roles affecting the cell performance. These structural properties are closely related to the exciton diffusion, dissociation of charge carriers and transport to the electrodes. The characterization of the structure to correlate with the processing control of a hierarchical structure of a planar heterojunction perovskite layer was, however, incomplete because of the limitations of conventional microscopes (i.e. scanning electron microscope and atomic-force microscope) and X-ray diffraction (XRD). For instance, XRD typically provides limited information because of the existence of preferential orientation of the perovskite grains.

To extend the current structural observations, simultaneous small-angle scattering and wide-angle X-ray scattering at grazing incidence (GISAXS/GIWAXS) techniques are an effective tool to probe quantitatively the hierarchical structure of a phase-separated bulk heterojunction structure in polymer solar cells. In particular, GIWAXS with a two-dimensional (2D) detector can provide sufficient information about crystallinity, including the orientation of all perovskite grains inside the film. Cheng-Si Tsao (Institute of Nuclear Energy Research), U-Ser Jeng (NSRRC) and Chun-Jen Su (NSRRC) cooperatively performed synchrotron-based X-ray-scattering techniques at **BL23A1** to probe quantitatively the hierarchical structure of planar heterojunction perovskite solar cells. The correlation between the crystallization behavior, crystal orientation, internal structure on nano- and meso-scales and surface morphology of the perovskite film as functions of various processing control parameters was discussed.

In Tsao's work, synchrotron GISAXS/GIWAXS measurements were simultaneously performed to characterize quantitatively the multi-length-scale structures of bulk $CH_3NH_3PbI_{3-x}Cl_x$ perovskite films prepared under varied control conditions under (1) sequential vacuum deposition and (2) one-step solution-processed deposition.[1] In the one-step solution-processed deposition method, the evolution of an hierarchical pore-network structure inside the perovskite film into a dense grain structure (no internal pore) with a fractal surface was tuned with preparation parameters. In the sequential vacuum deposition method, a quantitative GISAXS analysis revealed how a fractal surface of densely aggregated grains evolves into a film on tuning the substrate temperature. The corresponding GIWAXS patterns demonstrated the variation of the orientation of crystalline grains and a phase transformation.

For $CH_3NH_3PbI_{3-x}Cl_x$ perovskite films prepared with sequential vacuum deposition, the critical parameter controlling the PCE and film structure is the substrate temperature for the vapor deposition of CH_3NH_3I onto the $PbCl_2$ film. The $CH_3NH_3PbI_{3-x}Cl_x$ perovskite films prepared at substrate temperatures 65, 75 and 85 °C were investigated with the simultaneous synchrotron GISAXS/GIWAXS measurements. Figure 1 shows the GISAXS profiles, $I(Q)$, of the vacuum-deposited $CH_3NH_3PbI_{3-x}Cl_x$ films at substrate temperatures 65, 75 and 85 °C, respectively. The GISAXS profiles show the behavior of a power-law scattering with the characteristic of surface fractal ($I(Q) \propto Q^{-\alpha}$; $3 \le \alpha \le 4$). The exponent α is related to the surface fractal dimension D_s according to $D_s = 6-\alpha$. The surface fractal

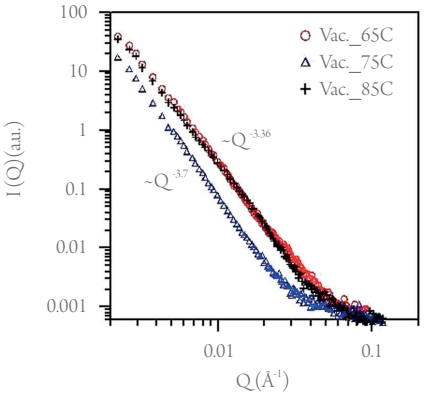

Fig. 1: GISAXS profiles of vacuum-deposited films of $CH_3NH_3PbI_{3-x}Cl_x$ prepared at substrate temperatures 65, 75 and 85 °C, respectively. [Reproduced from Ref. 1]